Design of Circular Polarized Antenna Using Gammadion Chiral Metamaterial as Linear-to-Circular Polarization Transformer

Preet Kaur[1, *] and Pravin R. Prajapati[2]

Abstract—The application of gammadion chiral metamaterial for converting linearly polarized waves to circularly polarized waves is presented in this paper. First of all, a traditional rectangular microstrip patch antenna has been designed at resonance frequency of 5.15 GHz, which gives linear polarization. The linearly polarized waves are allowed to feed gammadion chiral metamaterial, which is placed at a height of 33 mm above the reference antenna. The gammadion chiral metamaterial produces two special effects that are responsible for polarization rotation: circular dichroism and optical activity. As a result of these effects, the necessary conditions for circularly polarized radiation are fulfilled, and linear antenna is converted to the circularly polarized antenna. This method gets rid of designing of complicated feeding structure that is necessary for circular polarization. The role of gammadion chiral metamaterial to convert linear polarization to circular polarization has been described. The antenna is fabricated, and the measurement of return loss, axial ratio, radiation patterns, etc. is also carried out. Simulation and measurement results agree with each other.

1. INTRODUCTION

Nowadays, in an era of high speed communication, circularly polarized (CP) antennas have gained much attention in high speed advanced communication domain because of their special properties, which are not available with linearly polarized (LP) waves. Circularly polarized radiated waves have special characteristics such as better mobility, i.e., it provides nearly no any adverse effect due to misalignment angle between transmitting antenna and receiving antenna, reduction in the loss caused by multi-path effects, weather penetration, and less risk of bad weather conditions than linearly polarized waves, better signal strength through obstacles, etc. Because of the above features of CP antennas, it has been used for various purposes like global navigation satellite system, satellite communications, wireless sensors, wire-less power transmission, radio frequency identification, etc. for decades [1].

Several feeding techniques and embedding of slots have been reported to design a CP microstrip antenna, such as sequential rotation feeding technique [2], eight curved slots [3], fractal geometries [4], combining two LP and omnidirectional antennas with 90° phase difference on their terminal [5], helix and rectangle shape slots [6], sequentially rotated serial feed feeding network [7], Wilkinson power divider [8], quad-feed network [9], and aperture coupled [10]. The main disadvantage of all of these techniques is that one has to design the complex feeding mechanism and to embed complex slots on radiating elements to generate two degenerate orthogonal modes of equal amplitude and 90° phase difference/delay, which are two necessary conditions for CP radiation. The above said conventional designing methods make feeding mechanism complex and fabrication of the CP antenna difficult.

Recently, chiral media have provided new approaches for different applications such as sensor [11], cross-polarization conversion [12], right hand circular polarization to left hand circular polarization

* Corresponding author: Preet Kaur (preetmoar@gmail.com).
[1] Department of Electronics Engineering, J.C. Bose University of Science and Technology, Faridabad, Haryana, India. [2] Department of Electronics & Communication, A. D. Patel Institute of Technology, Gujarat, India.

conversion and vice versa [13], asymmetric transmission [14] due to their exotic EM properties (discussed in Section 2), which are not available in nature. This paper demonstrates the use of chiral metamaterial (CMM) as linear-to-circular polarization transformer without the use of complicated feeding mechanism and complex design of slots, which are generally used in traditional techniques.

2. THE PHYSICAL PROPERTIES OF CHIRAL METAMATERIALS

Chiral metamaterials geometrical structure does not have mirror symmetry in any plane. The CMM structure is asymmetrical in design. Due to this orientation, CMM produces two important characteristics. One is the circular dichroism property [15], and the other is optical activity [16]. Circular dichroism property provides different absorptions to right hand circularly polarized (RHCP) and left hand circularly polarized (LHCP) radiated waves when it passes through chiral metamaterial. Optical activity property is a performance parameter of the CMM, which represents how much the rotation of the polarization plane of an LP wave done when propagating through CMM. Different absorptions of LHCP and RHCP waves inside the CMM are due to different refractive indices offered to LHCP and RHCP waves.

The transmission coefficients of incident wave passing through CMM depend on the polarization. Chiral metamaterial has optical activity and circular dichroism effect as per the relationship [16] given below,

$$D = \varepsilon\varepsilon_0 E + j\kappa\sqrt{\varepsilon_0\mu_0}H \tag{1}$$

$$B = -j\kappa\sqrt{\varepsilon_0\mu_0}E + \mu\mu_0 H \tag{2}$$

where B = Magnetic flux density, D = Electric flux density, ε_0 = permittivity of vacuum, μ_0 = permeability of vacuum, ε = relative permittivity the chiral medium, μ = relative permeability of the chiral metamaterial, κ = chirality parameter. Chirality parameter (κ) is dimensionless, and it demonstrates the cross coupling effect between magnetic and electric fields [17]. Due to chirality parameter, CMM offers different refractive indices (n) to LHCP and RHCP waves. The relationship between chirality parameter and refractive indices of LHCP ($-$) and RHCP ($+$) waves is given as follows

$$n_\pm = n \pm \kappa \tag{3}$$

If chirality parameter is large enough, refractive index for one wave either LHCP or RHCP becomes negative. So, when LHCP and RHCP waves pass through CMM, it offers a different transmission coefficient to both waves and allows to pass one wave, while suppresses the other. The linearly polarized wave is a combination of LHCP wave and RHCP wave, and it is given by,

$$\text{LP} = \frac{1}{2}\text{LHCP} + \frac{1}{2}\text{RHCP}$$

To obtain CP wave from the LP wave, either of the LHCP or RHCP wave should be small. Due to circular dichroism property of CMM, LP wave after passing through CMM one wave (LHCP or RHCP) is suppressed, and LP wave changes into circular polarization. Azimuth rotation angle (θ) and ellipticity (η) are the parameters that characterize the amplitude and phase difference of LHCP and RHCP waves when LP wave passes through CMM. Azimuth rotation angle and ellipticity are given by following equations [18, 19],

$$\theta = \frac{1}{2}\left[\arg(T_{++}) - \arg(T_{--})\right] \tag{4}$$

$$\eta = \arctan\left(\frac{|T_{++}| - |T_{--}|}{|T_{++}| + |T_{--}|}\right) \tag{5}$$

where T_{++} = transmission coefficients for RHCP waves, T_{--} = transmission coefficients for LHCP waves. Ellipticity (η) represents the differential absorption of RHCP and LHCP waves because of circular dichroism in CMM. Gammadion chiral metamaterial (GCMM) used in this paper is printed on the both sides of the substrate. GCMM is designed in such a way that when LP wave passes through it radiates the LHCP wave and absorbs the RHCP wave, converting the LP wave into CP wave.
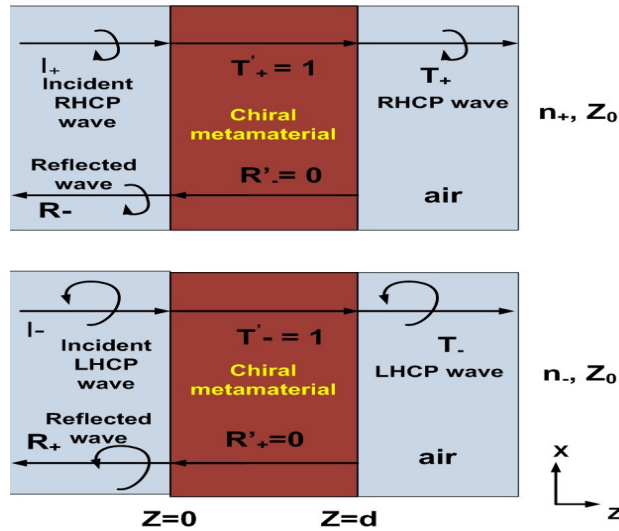
Figure 1. Schematics of chiral behavior in terms of transmission and reflection coefficients of RHCP and LHCP waves (T'_+ & T'_- are transmission coefficients of CMM towards RHCP and LHCP respectively, R'_- & R'_+ are reflection coefficients of CMM towards RHCP and LHCP respectively) [20].

To explain the CMM behavior towards the transmission and reflection coefficients of LHCP and RHCP radiating waves, a CMM slab placed in air is shown in Fig. 1. As per the phenomena described in Fig. 1, after applying the boundary condition of tangential E and H fields at two boundaries of CMM (i.e., $z = 0$ and $z = d$), the absorbing and reflection behaviors of chiral metamaterial for integral part of linear wave, i.e., LHCP and RHCP waves, can be understood.

3. LINEARLY POLARIZED PATCH ANTENNA DESIGN AND RESULTS

First of all, the reference rectangular planar antenna is designed without embedding the slots, so only LP waves can be generated. An inexpensive FR4 substrate with a dielectric constant of 4.4, size of $70 \times 70 \, \text{mm}^2$, loss tangent of 0.0025, and thickness of 1.524 mm is considered as the base substrate. The traditional microstrip feed is used here. Inside cut is embedded at the junction of microstrip feed and rectangular patch to improve impedance matching. Fig. 2(a) shows the reference patch antenna design with its geometric parameters, and Fig. 2(b) presents the fabricated reference patch antenna.

The reflection coefficient (S_{11}) of the reference antenna has been measured on vector network analyzer (VNA). Fig. 3 shows that according to simulation result, the patch antenna has a centre resonant frequency at 5.15 GHz with S_{11} of -14.069 dB, while in measurement S_{11} of -12.89 dB is obtained. The simulated result of axial ratio (AR) of the reference rectangular patch antenna is shown in Fig. 4(a). It can be concluded that at the resonance frequency of 5.15 GHz, the AR of 45.76 dB is obtained, which shows that the reference rectangular patch antenna is linearly polarized. Fig. 4(b) presents the LHCP and RHCP gains of linearly polarized reference rectangular patch antenna. As the reference antenna radiates LP waves, the individual components of LHCP and RHCP of electromagnetic wave has the same value of the gain. Around 0.9 dB gains of both components have been achieved in simulation.

4. DESIGN AND RESULTS OF UNIT CELL OF GAMMADION CMM

The unit cell of GCMM is printed on both sides of the substrate of FR4 as demonstrated in Fig. 5. All design dimensions of the reference rectangular antenna and CMM are optimized using HFSS software V. 2017. To design and simulate the CMM in HFSS, periodic boundary conditions are applied in the x and y directions, and Floquet ports are applied in z direction. All the optimized design parameters of
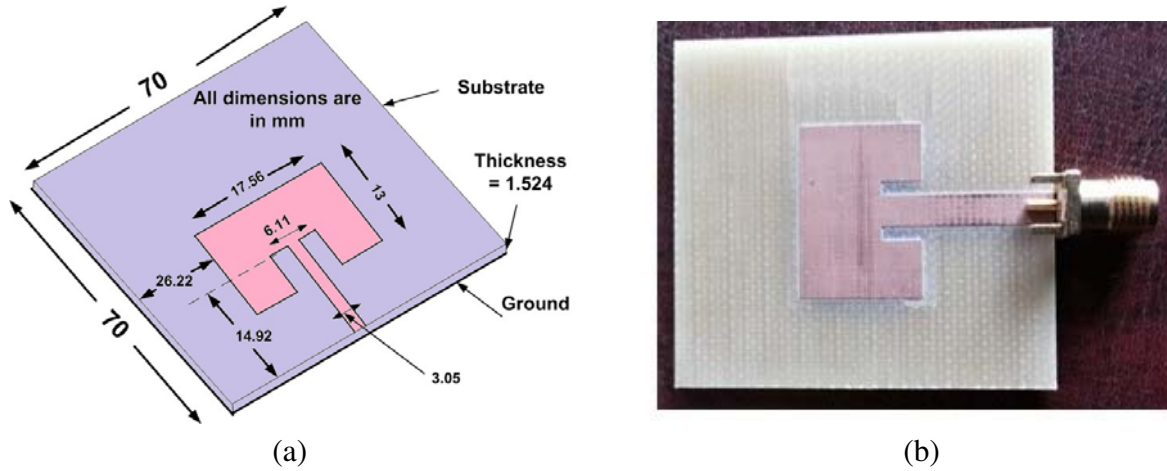
Figure 2. (a) Geometry of the reference rectangular patch antenna (all dimensions are in mm), (b) fabricated reference microstrip patch antenna.
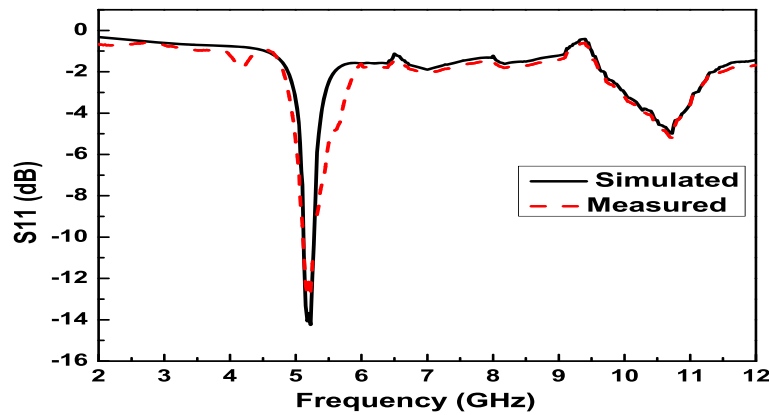

Figure 3. Comparison of the simulation and measurement results of reflection coefficient (S_{11}).
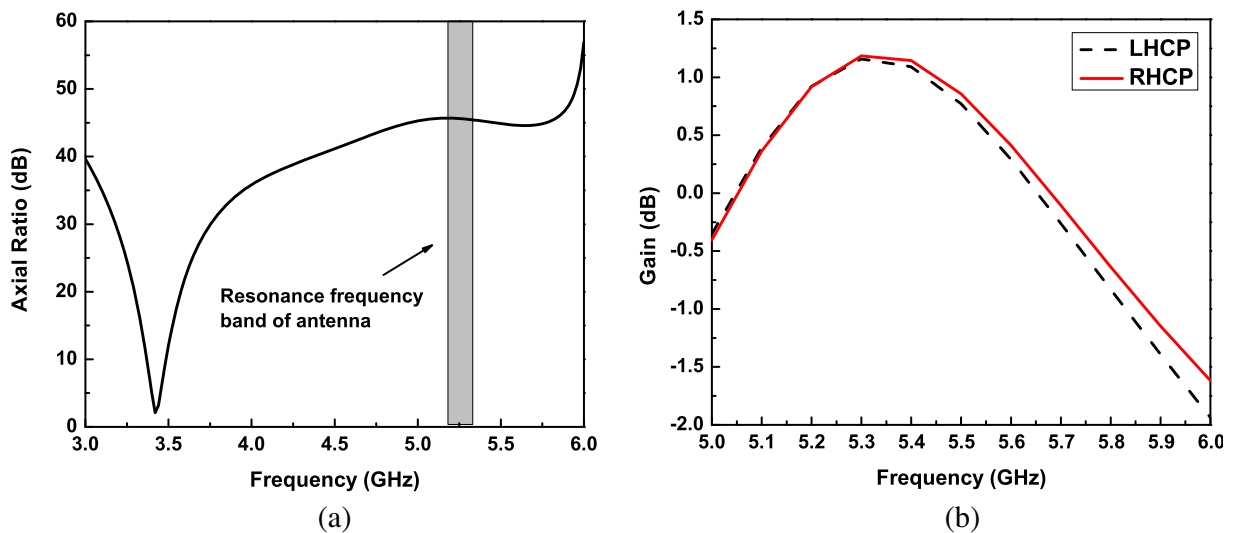

Figure 4. (a) Simulated result of AR of the reference antenna, (b) simulated results of LHCP and RHCP gain of the reference rectangular patch antenna.
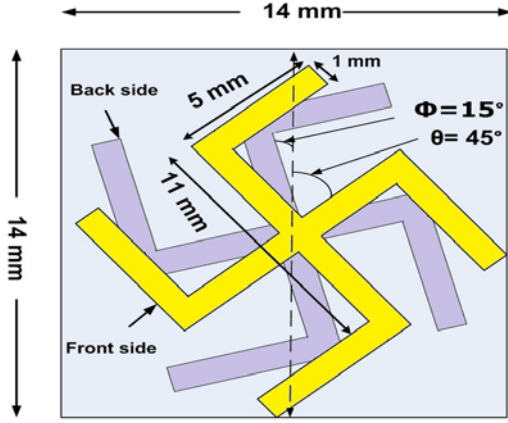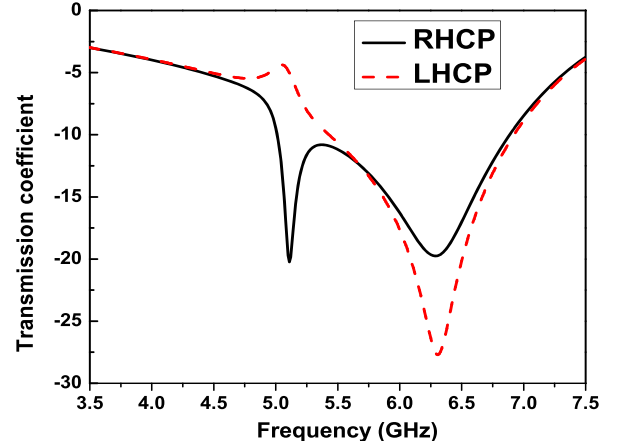
Figure 5. Single cell of GCMM.

Figure 6. Simulated transmission coefficients of LHCP and RHCP waves after passing through GCMM.

GCMM are shown in Fig. 5.

LP waves are allowed to pass through GCMM. Practically, it is a bit difficult to measure the reflection and transmission coefficients directly for radiated CP waves from GCMM. The calculation of these coefficients $(T_{++}, T_{+-}, T_{-+}, T_{--})$ is possible from the transmission and reflection coefficients $(T_{xx}, T_{xy}, T_{yx}, T_{yy})$ of linearly polarized waves, which represents the effect produced by the proposed gammadion CMM. The numerical relation between the coefficients of CP and LP waves is given by [21, 22].

$$
\begin{pmatrix} T_{++} & T_{+-} \\ T_{-+} & T_{--} \end{pmatrix} = \begin{pmatrix} (T_{xx} + T_{yy}) - i\,(T_{xy} - T_{yx}) & (T_{xx} - T_{yy}) + i\,(T_{xy} + T_{yx}) \\ (T_{xx} - T_{yy}) - i\,(T_{xy} + T_{yx}) & (T_{xx} + T_{yy}) - i\,(T_{xy} + T_{yx}) \end{pmatrix} \tag{6}
$$

The transmission coefficients of the RHCP (T_{++}) and LHCP (T_{--}) waves after getting over through GCMM are given in Fig. 6 as a function of frequency (the cross coupling transmission, T_{-+} and T_{+-} are not shown here because their amplitudes are almost negligible).

As a result of the asymmetric geometry of CMM in the direction of propagation of the radiated waves, the transmission responses for RHCP and LHCP divide into two curves. It is observed that two resonance peaks are achieved at frequencies $f = 5.15\,\text{GHz}$ and $6.25\,\text{GHz}$, in T_{++} and T_{--} curves. At 5.15 GHz, transmission coefficient of RHCP (T_{++}) is significantly deeper than LHCP (T_{--}) which means that GCMM passes the LHCP waves and suppresses the RHCP waves.

The simulated results of the azimuth rotation angle (θ) and ellipticity (η) are presented in Fig. 7(a). At a center frequency of 5.15 GHz, after passing from CMM, the radiated waves have a change of ellipticity 45° and a change of azimuth rotation angle 180°. Ellipticity $(\eta) = 45°$ and change of azimuth rotation angle $(\theta) = 180°$ correspond to pure CP radiating wave, while $\eta = 0°$ represents the LP wave [23]. Hence, designed CMM converts the LP waves into CP waves. Fig. 7(b) shows the variation of chirality parameter (κ) of gammadion chiral metamaterial with respect to frequency. From the graph, it can be seen that chirality parameter is negative in the frequency range of 4.8 GHz to 5.3 GHz. Because of the negative chirality parameter, it offers different refractive indices and different transmission coefficients to LHCP and RHCP waves as per Equation (6). This is also clear from the transmission coefficient characteristics mentioned in Fig. 6 that the designed GCMM allows LHCP wave to radiate and suppress the RHCP wave.

4.1. Design of Patch Antenna with GCMM Cover

GCMM cover is kept over the reference patch antenna to convert linearly polarized waves to circular waves. For this, on the substrate of FR4, an array of 5×5 unit cells of GCMM is printed on both sides of this substrate as demonstrated in Figs. 8(a), (b) and placed over the reference patch antenna

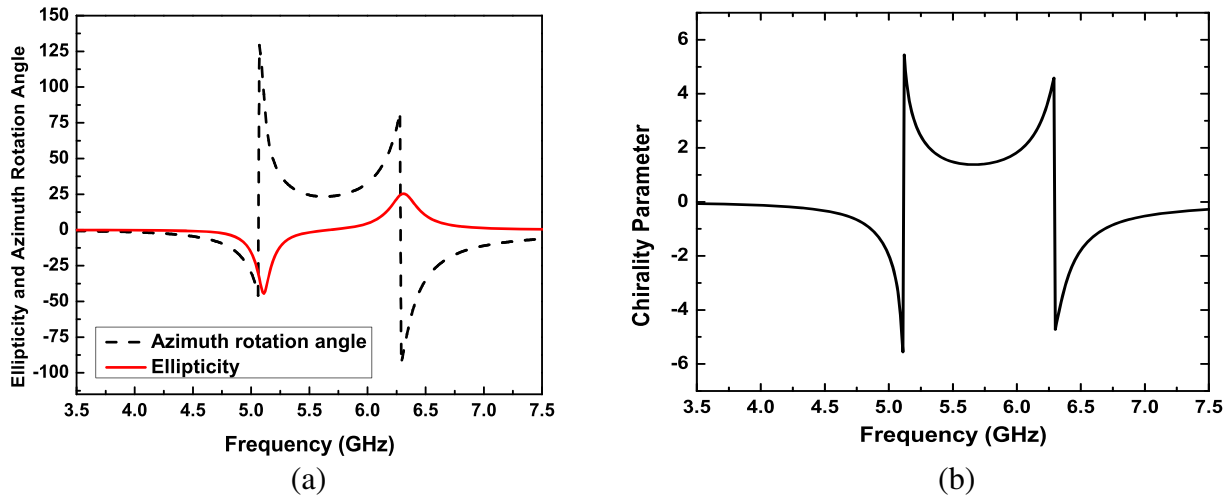(a)   (b)

Figure 7. (a) Effect of the CMM on radiating waves in terms of the ellipticity and azimuth rotation angle, (b) chirality parameter (κ) of GCMM.

(a)   (b)

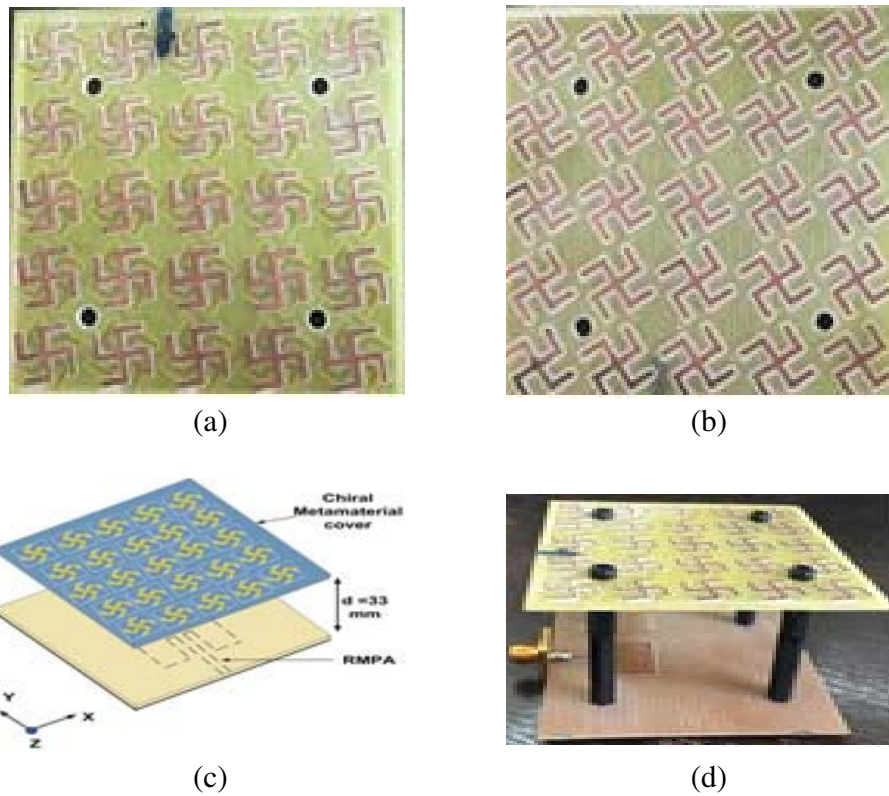(c)   (d)

Figure 8. (a) Top layer of GCMM, (b) bottom layer of GCMM, (c) exploded view of proposed patch antenna with GCMM cover, (d) proposed fabricated patch antenna.

at a distance of 33 mm. Because of the periodic arrangement of gammadion structure, it behaves like a metamaterial. Fig. 8(c) shows the exploded view of the proposed patch antenna with GCMM cover. The distance between reference patch antenna and GCMM cover is optimized using HFSS software V. 2017.
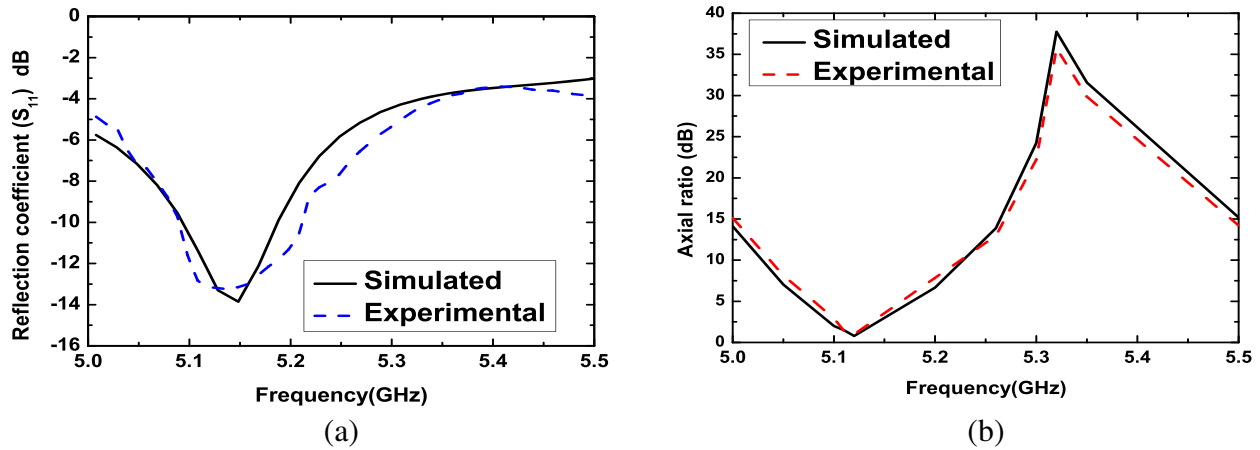
Figure 9. (a) Comparison of simulated and measured results of reflection coefficient (S_{11}), (b) simulated and measured results of AR of the proposed antenna with GCMM cover.
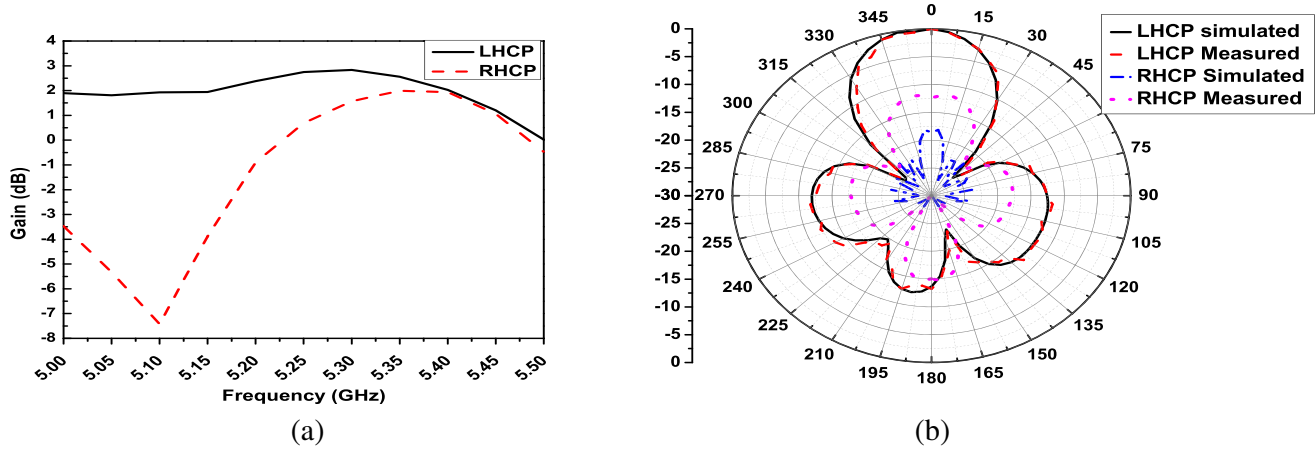

Figure 10. (a) LHCP and RHCP gain of the proposed antenna with GCMM cover, (b) radiation pattern of proposed antenna with GCMM cover at 5.15 GHz frequency and in $\phi = 0°$ plane.

5. RESULT & DISCUSSION OF PATCH ANTENNA WITH GCMM COVER

The fabricated prototype shown in Fig. 8(d) is tested using 20 GHz Rohde and Schwarz make VNA (Model No. 1127.8500 ZVM) for the measurement of bandwidth and to find the resonance frequency of the antenna. To minimize the errors, VNA was calibrated for a desired frequency range before testing. The comparison of measured reflection coefficient graph along with the simulated reflection coefficient is shown in Fig. 9(a). The proposed antenna resonates at 5.15 GHz frequency. From this result, it is concluded that simulated and measured results are almost same.

It is concluded that according to Fig. 6, the radiated wave is CP at 5.15 GHz frequency, which is also justified by Fig. 9(b) which shows that the value of AR is 1.01 dB in simulation and 1.2 dB in measurement. Fig. 10(a) demonstrates the LHCP and RHCP gains of the proposed antenna. LHCP gain is nearly 2 dB, and RHCP gain is −7.5 dB, which also shows that the antenna is left hand circularly polarized.

For measurement of radiation patterns and AR, an anechoic chamber was used. Fig. 10(b) presents the simulated and measured radiation patterns of the proposed antenna for LHCP wave. The RHCP gain of the antenna with CMM cover is about 5.8 dB higher than its LHCP gain in the boresight direction. Also, the placement of CMM cover on the antenna causes the half power beamwidth (HPBW)

to decrease from 70° to 44° and the side lobe level (SLL) to increase from −20.31 dB to −12.43 dB. Simulated and measured radiation patterns are in close agreement. The proposed patch antenna has very simple design and uses a simple technique to convert LP wave to CP instead of using a complicated feeding network/method.

As a further investigation and to understand the mechanism of the polarization conversion by CMM, we investigated the E field and H field associated with CMM and distributed on top and bottom copper layers. Through careful analysis of Fig. 11, it is observed that prime concentration of the magnetic field is available around the proposed GCMM, which gives the confirmation of asymmetric resonance mode. Upper and bottom CMMs act as magnatic dipole. The asymmetric resonance mode is excited by the magnetic dipoles. In addition to this, the electric field distribution concentrated near the CMM at 5.15 GHz validates the symmetric current. This is created by the coupling of the electric dipoles [24]. Due to the proximity of the electric and magnetic resonant frequencies, the chirality parameter at resonance frequency is increased. Therefore, very special characteristics of chiral, i.e., optical activity and circular dichroism have been achieved [25].
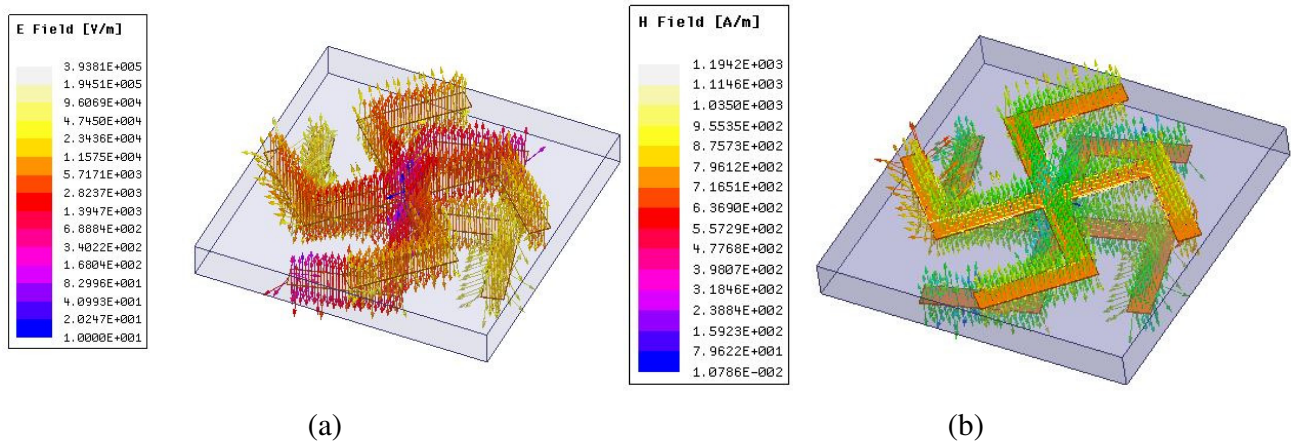

| (a) | (b) |

Figure 11. (a) Electric field pattern at CMM at the resonant frequency of 5.15 GHz, (b) magnetic field pattern at CMM at the resonant frequency of 5.15 GHz.

Table 1 shows the performance comparison of the proposed technique with earlier reported techniques. As per this comparison, it is concluded that the design and fabrication of our proposed technique is simple and gives more polarization purity, i.e., AR value is near an ideal value, i.e., 0 dB.

Table 1. Comparison of proposed technique with earlier reported techniques with respect to design flexibility and performance.

Ref. no.	Feeding used	AR (dB)	Technique used to obtained CP radiation
[3]	Coaxial probe	1.71	Embedding eight curved slots
[4]	Coaxial probe	1.2	Fractal boundaries
[5]	Coaxial probe	1.3	Combining two LP and omnidirectional antennas with 90° phase difference
[6]	Coaxial line	2.5	Helix and rectangle shape slots
[7]	Through probes	2.05	Sequentially rotated serial feed feeding network
Proposed technique	Microstrip line	1.02	Gammadion chiral metamaterial

6. CONCLUSION

The application of gammadion chiral metamaterial as polarization rotator has been presented, and this is also confirmed by different simulations and experiments that have been carried out. Using circular dichroism effect of GCMM, a circularly polarized antenna for Wi-Fi application has been proposed. The proposed CP patch antenna resonates at 5.15 GHz with an axial ratio of 1.02 dB and has good polarization purity. Our investigation enriches the asymmetric transmission effect and chiral behavior of gammadion structure. The proposed asymmetric GCMM antenna and technique could give more insight in the field of advanced communication systems. The advantage of this technique over traditional technique is that it does not use a complex feeding mechanism and provides a simple antenna structure. By selecting materials having low loss and low dielectric constant such as Roger's substrate (RO3003), the conversion and radiation efficiency can be further improved. Reconfigurable polarization rotator, which gives a additional feature of the polarization control, can be the future prolongation of this research work.

REFERENCES

1. Gao, S., Q. Luo, and F. Zhu, *Circular Polarized Antenna*, Wiley Publication, U.K., 2014.
2. Caso, R., A. Michel, M. Rodriguez-Pino, and P. Nepa, "Dual-band UHF-RFID/WLAN circularly polarized antenna for portable RFID readers," *IEEE Trans. on Antennas and Propag.*, Vol. 62, 2822–2826, 2014.
3. Yu, D., S. Gong, Y. Wan, and W. Chen, "Omnidirectional dual-band dual circularly polarized microstrip antenna using TM01 and TM02 modes," *IEEE Antennas and Wireless Propag. Lett.*, Vol. 13, 1104–1107, 2014.
4. Oraizi, H. and S. Hedayati, "Miniaturization of microstrip antennas by the novel application of the giuseppe peano fractal geometries," *IEEE Trans. on Antennas and Propag.*, Vol. 60, 3559–3567, 2012.
5. Wu, J. and K. Sarabandi, "Compact omnidirectional circularly polarized antenna," *IEEE Trans. on Antennas and Propag.*, Vol. 65, 1550–1557, 2017.
6. Zheng, G. and B. Sun, "High gain normal mode omnidirectional circularly polarized antenna," *IEEE Antennas and Wireless Propag. Lett.*, Vol. 17, 1104–1108, 2018.
7. Fartookzadeh, M. and S. H. Mohseni Armaki, "Circular feeding network for circular polarisation reconfigurable antennas," *Electron. Lett.*, Vol. 55, 677–679, 2019.
8. Lin, Y. F., H. M. Chen, C. H. Chen, and C. H. Lee, "Compact shorted inverted L antenna with circular polarisation for RFID handheld reader," *Electro. Lett.*, Vol. 49, 442–449, 2013.
9. Liu, Q., Y. Liu, Y. Wu, M. Su, and J. Shen, "Compact wideband circularly polarized patch antenna for CNSS applications," *IEEE Antennas and Wireless Propag. Lett.*, Vol. 12, 1280–1283, 2013.
10. Lai, H. W., K. M. Mak, and K. F. Chan, "Novel aperture-coupled microstrip-line feed for circularly polarized patch antenna," *Progress In Electromagnetics Research*, Vol. 144, 1–9, 2014.
11. Bakir, M., M. Karaaslan, O. Akgol, and C. Sabah, "Multifunctional metamaterial sensor applications based on chiral nihility," *Opt. Quant. Electron.*, Vol. 49, 346–363, 2017.
12. Fan, J. and Y. Cheng, "Broadband high-efficiency cross-polarization conversion and multifunctional wavefront manipulation based on chiral structure metasurface for terahertz wave," *J. Phys. D: Appl. Phys.*, Vol. 53, 2020.
13. Cheng, Y., J. Fan, H. Luo, and F. Chen, "Dual band and high-efficiency circular polarization convertor based on anisotropic metamaterial," *IEEE Access*, Vol. 8, 7615–7621, 2020.
14. Cheng, Y., H. Luo, F. Chen, X. Mao, and R. Gong, "Photo-excited switchable broadband linear polarization conversion via asymmetric transmission with complementary chiral metamaterial for terahertz waves," *OSA Continuum*, Vol. 2, 2391–2400, 2019.
15. Cheng, Y., Y. Nie, L. Wu, and R. Z. Gong, "Giant circular dichroism and negative refractive index of chiral metamaterial based on split-ring resonators," *Progress In Electromagnetics Research*, Vol. 138, 421–432, 2013.

16. Hu, Y., Y. Wang, L. Liang, Y. He, W. Chen, and Z. Yan, "Study on circularly polarized patch antenna with asymmetric chiral metamaterial," *IEEE Antennas and Wireless Propag. Lett.*, Vol. 17, 907–910, 2018.

17. Akgol, O., E. Unal, O. Altintas, M. Karaaslan, F. Karadag, and C. Sabah, "Design of metasurface polarization converter from linearly polarized signal to circularly polarized signal," *Optik*, Vol. 161, 12–19, 2018.

18. Fang, F., Y. Cheng, and H. Liao, "Giant optical activity and circular dichroism in the terahertz region based on bi-layer Y-shaped chiral metamaterial," *Optik — Int. J. Light Electron. Opt.*, Vol. 125, 6067–6070, 2014.

19. Cheng, Y., W. Li, and X. Mao, "Triple-band polarization angle independent 90° polarization rotator based on fermat's spiral structure planar chiral metamaterial," *Progress In Electromagnetics Research*, Vol. 165, 35–45, 2019.

20. Li, Z., M. Mutlu, and E. Ozbay, "Chiral metamaterials: From optical activity and negative refractive index to asymmetric transmission," *J. of Optics*, Vol. 15, No. 2, 2013.

21. Dincer, F., C. Sabah, M. Karaaslan, E. Unal, M. Bakir, and U. Erdiven, "Asymmetric transmission of linearly polarized waves and dynamically wave rotation using chiral metamaterial," *Progress In Electromagnetics Research*, Vol. 140, 227–239, 2013.

22. Hu, Y. W., Y. Wang, Z. M. Yan, and H. C. Zhou, "A high-gain circularly polarized Fabry-Perot antenna with chiral metamaterial-based circular polarizer," *Microw. and Optical Technol. Lett.*, 1–6, 2019.

23. Cheng, Z, and Y. Cheng, "A multi-functional polarization convertor based on chiral metamaterial for terahertz waves," *Optics Communications*, Vol. 435, 178–182, 2019.

24. Zhou, J., J. Dong, B. Wang, T. Koschny, M. Kafesaki, and C. M. Soukoulis, "Negative refractive index due to chirality," *Phys. Rev. B*, Vol. 79, 121104–4, 2009.

25. Zarifi, D., M. Soleimani, V. Nayyeri, and J. Rashed-Mohassel, "On the miniaturization of semiplanar chiral metamaterial structures," *IEEE Trans. on Antennas and Propag.*, Vol. 60, No. 12, 5768–5776, 2012.